Available online at www.sciencedirect.com
ScienceDirect
Hearing Research 221 (2006) 104–118
Hearing Research
www.elsevier.com/locate/heares

Research paper

Synaptic alterations at inner hair cells precede spiral ganglion cell loss in aging C57BL/6J mice

Sofia Stamataki, Howard W. Francis *, Mohamed Lehar, Bradford J. May, David K. Ryugo

Department of Otolaryngology-Head and Neck Surgery, Johns Hopkins University, 720 Rutland Avenue, Baltimore, MD 21205, United States

Received 24 May 2006; received in revised form 22 July 2006; accepted 26 July 2006
Available online 26 September 2006

Abstract

Hearing deficits have often been associated with loss of or damage to receptor hair cells and/or degeneration of spiral ganglion cells. There are, however, some physiological abnormalities that are not reliably attributed to loss of these cells. The afferent synapse between radial fibers of spiral ganglion neurons and inner hair cells (IHCs) emerges as another site that could be involved in transmission abnormalities. We tested the hypothesis that the structure of these afferent terminals would differ between young animals and older animals with significant hearing loss. Afferent endings and their synapses were examined by transmission electron microscopy at approximately 45% distance from the basal end of the cochlea in 2–3 month-old and 8–12 month-old C57BL/6J mice. The number of terminals in older animals was reduced by half compared to younger animals. In contrast, there was no difference in the density of SGCs between the age groups. Older animals featured enlarged terminals and mitochondria and enlarged postsynaptic densities and presynaptic bodies. These morphological changes may be a combination of pathologic, adaptive and compensatory responses to sensory dysfunction. Improved knowledge of these processes is necessary to understand the role of afferent connectivity in dysfunction of the aging cochlea.

Keywords: Cochlea; Afferent innervation; Synapse; Ultrastructure; Presbycusis

1. Introduction

Changes at the interface between receptor cells and afferent endings represent a poorly understood stage in the progression of hearing dysfunction associated with presbycusis. It is now well established that loss of radial fibers can exceed the loss of spiral ganglion cell bodies in human cases of presbycusis (Chen et al., 2006; Nadol, 1979; Pauler et al., 1986; Spoendlin and Schrott, 1988, 1990). A distal-to-proximal gradient of radial fiber loss has also been observed in C57BL/6J mice (White et al., 2000), a laboratory animal model that exhibits patterns of hearing loss and cochlear degeneration comparable to human presbycusis (Francis et al., 2003; Henry and Chole, 1980; Hequembourg and Liberman, 2001; Li and Borg, 1991). Alterations in sensory–neural synaptic structure that precede or follow denervation may hold the key to understanding the mechanisms of afferent cochlear pathology. Since auditory information is conveyed to the brain by the pattern of action potentials in the auditory nerve, rearrangement and/or degradation of synaptic components at this location will affect the encoding process. Corruption of transmission through the IHC-afferent fiber synapse would disturb the fidelity of spike timing represented within the auditory nerve and change the very signals upon which speech understanding ultimately depends.

Synaptic alterations have been documented in the aging central nervous system where a reduction in cortical synaptic density and increase in synaptic size are associated with cognitive decline in humans (Bertoni-Freddari and Fattoretti, 1989) and senescence in laboratory animals (Bertoni-Freddari et al., 1996). Changes in the proportion of

* Corresponding author. Present address: Department of Otolaryngology-Head and Neck Surgery, Johns Hopkins University, 601 N. Caroline Street, Johns Hopkins Outpatient Center, 6th Floor, Baltimore, MD 21287, United States. Tel.: +1 410 955 1640; fax: +1 410 614 8610.
E-mail address: hfrancis@jhmi.edu (H.W. Francis).

0378-5955/$ - see front matter © 2006 Elsevier B.V. All rights reserved.
doi:10.1016/j.heares.2006.07.014

low- and high-spontaneous rate fibers were observed in cats with noise-induced hearing loss (Liberman and Dodds, 1984), congenital hearing loss (Ryugo et al., 1998), and gerbils with age-induced hearing loss (Schmiedt et al., 1996). Because specific ultrastructural features are associated with discharge properties of auditory nerve fibers (Liberman and Dodds, 1984), they may exhibit alterations that accompany specific physiological changes.

On the basis of these considerations, we conducted a morphometric study of the innervation of IHCs in the C57BL/6J mouse at two ages with known differences in hearing sensitivity. We tested the hypothesis that the structure of afferent terminals and their synapses with IHCs is different between young adult and older animals, and argue that the observed changes in synaptic organization represent part of the substrate underlying age-related hearing loss.

2. Materials and methods

2.1. Animals

Female C57BL/6J mice with documented dates of birth were obtained from Jackson Laboratories. Three mice were studied at 2–3 months of age (the younger group) and three were studied at 8–12 months of age (the older group). No outer or middle ear pathology was encountered in any of the animals studied. All procedures were conducted in accordance with an animal protocol approved by the Animal Care and Use Committee at the Johns Hopkins University School of Medicine.

2.2. Hearing assessment

Hearing thresholds were measured in five mice using auditory brainstem responses (ABR) as previously described (Rivas and Francis, 2005). Evoked potentials were recorded in anesthetized mice using $Ag/AgCl^{-}$ electrodes on the neck (ground), vertex, and over the bulla of the experimental ear. The ABR was based on the average of 500–1000 evoked responses to calibrated pure tones, which were presented at intensity increments of 5 dB sound pressure level to generate the input–output functions presented in the bottom panels of Fig. 1. Response magnitude was calculated as the maximum peak-to-peak voltage during a 5–10-ms time window that began 2.5 ms after stimulus onset (Fig. 1). Baseline noise levels were similarly measured during the final 15–20-ms window of the response. The threshold was defined as the presentation level that evoked a response with amplitude equal to or exceeding 2 standard deviations (SD) above the mean baseline noise level for that stimulus condition (Fig. 1, top panels).

2.3. Cochlear tissue processing

Intracochlear perfusion of fixatives was performed while the animal was deeply anesthetized after ABR measurements (Francis et al., 2004, 2003). The middle ear was entered through a post-auricular incision and visualized using an operating microscope. The cochlear apex was fenestrated with a pick to facilitate the flow of fixative. The stapes and its footplate were removed from the oval window through which a solution of 1% OsO_4 and 1% potassium ferricyanide $[FeK_3(CN)_6]$ was slowly perfused using a Pasteur pipette with a tightly fitting flamed tip for 3–5 min. The animal was then decapitated and cochlear perfusion was resumed through both oval and round windows for an additional 5–10 min. The appearance of a dark stripe representing the lateral wall of the cochlea indicated a successful perfusion. Respiration was monitored throughout the procedure until decapitation. If labored breathing was observed during the perfusion, the animal was immediately decapitated, the bulla widely opened and perfusion resumed. The heads were then submerged in the osmium solution for an additional 45 min prior to the removal of the temporal bones. Because optimal fixation of afferent terminals was typically achieved in the first ear to be perfused (left ear), no attempt was made to prepare the contralateral ear for electron microscopy.

The cochleae were removed using fine tipped rongeurs, decalcified with 0.1 M EDTA (with 1% glutaraldehyde), dehydrated in graded alcohols and propylene oxide, and then embedded in Araldite (Francis et al., 2003; Hequembourg and Liberman, 2001). The cochleae were sectioned parallel to the modiolus at 40–50 μm thickness and mounted between sheets of Aclar for light microscopic analysis. The cochlear spiral was reconstructed at the junction of the inner and outer pillar cells using NIH Image, Voxblast (Vaytech, Inc) and Neurolucida (Microbrightfield, Inc., Essex, VT).

2.4. Ultrastructural study of afferent innervation

Morphological analyses were conducted in the same cochlear region so as to minimize variability caused by differences in frequency location. The transitional zone between the normal organ of Corti and the region of complete loss in older animals was selected for analysis. This region allowed us to identify changes in IHC afferent structure associated with a full complement of OHCs in young mice compared with moderate loss of OHCs in older mice (Fig. 3). The length of the organ of Corti was normalized to 100% and the sample excised at 45% (±5%) of the cochlear length as measured from the basal end. This location corresponds to 22 kHz based on a published cochlear frequency map (Muller et al., 2005).

The tissue was embedded in a BEEM capsule and cut (75 nm thickness) approximately perpendicular to the long axis of the IHC (Francis et al., 2004, 2006). Ultrathin sections were placed in series on Formvar grids and stained with uranyl acetate. Electron micrographs were taken of every other section using a Jeol JEM-100CX II or Hitachi H-7600 microscope. Micrographs were digitized and the resulting images were aligned with a PC application called

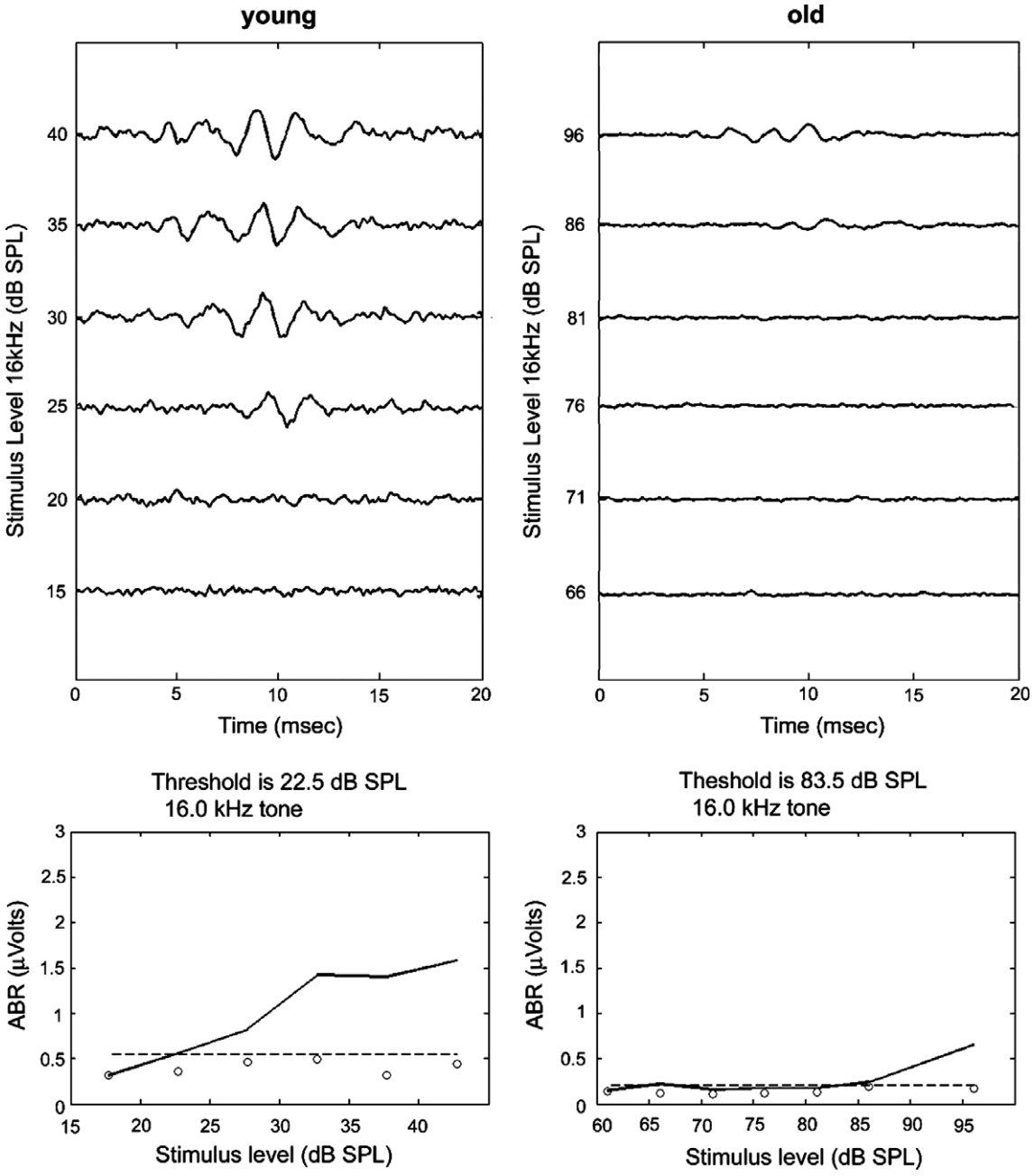

Fig. 1. Examples of ABR recordings at 16 kHz in a young (Y1) and an old (O1) C57BL/6J mouse (top). Maximum peak-to-peak amplitudes in ABR responses are compared to baseline noise amplitudes to determine threshold (bottom). The threshold is defined as the sound level at which ABR response amplitude (solid line) is 2 SD greater than baseline noise amplitudes (broken line). The higher thresholds in older animals are consistent with hearing loss.

Serial EM (SEM, using the absolute mode) available online at www.synapses.mcg.edu/lab/howto/mito.htm (Falia and Harris, 2001a). Profiles of inner hair cells, nerve endings, appositions, and membrane specializations were traced and stacked in series using Neurolucida (Microbrightfield, Inc., Essex, VT). Average section thickness was determined separately for each block of tissue using the minimal folds method (De Groot, 1988; Falia and Harris, 2001b) which was performed (De Groot, 1988; Falia and Harris, 2001b) randomly on every 10th section. Fold width was measured at its narrowest point in triplicate and halved to estimate section thickness. Mean section thickness ($\pm$SD) was measured as 74.2 ± 17.2 nm.

The number, size and morphologic features of afferent innervation were determined for 2–4 IHCs from each animal. Terminal volume, mitochondrial content and apposition area were calculated using the dimensions of profiles traced in alternate sections. The product of section interval and the sum of profile areas was used to estimate terminal and mitochondrial volumes. The sum of profile length was multiplied by section interval to estimate apposition area. Synaptic features were determined in similar fashion where

PSD area was calculated by multiplying the sum of PSD profile length and section interval, and SB surface area was calculated by multiplying the sum of SB profile perimeter and section interval. The number of clear vesicles making contact with the pre-synaptic membrane (docked) was counted and additional counts were made for vesicles found within 30- and 100-nm of the SB edge. The density of neurons within the spiral ganglion region that supplied IHCs under study was determined by a "blind" observer. This tissue was excised, embedded in Araldite and cut at 1 μm thickness. Ganglion cells with distinct nucleoli were counted within a randomly placed 50 μm square grid, and repeated 12–15 times in multiple sections for each specimen. Light microscopic analysis of the organ of Corti was also conducted in the frequency region of interest. Inner hair cell nuclei were counted within a known length of the basilar membrane to generate a density in cells per mm. As previously described (Francis et al., 2003) the percent loss of OHCs was estimated in the cochlear section under EM study and in flanking sections, from cell count decrements relative to Deiter cells with which there is a 1:1 relationship.

3. Results

Diminished hearing sensitivity in older animals was accompanied by partial OHC loss, whereas IHCs and SGCs were preserved. Available auditory brainstem response (ABR) measurements in two younger mice suggest normal to mildly reduced sensitivity in this age group and a significant elevation of thresholds in older animals (Table 1, Fig. 1). Light microscopic examination of the cochlear region that was subsequently studied with an electron microscope revealed comparable densities of IHCs (younger group 121.6 ± 19.3 cells/mm; older group 93.7 ± 10.8 cells/mm) and SGCs (younger group 3.073 ± 0.184 (10^{-3}) cells/μm^2; older group 3.155 ± 0.121 (10^{-3}) cells/μm^2) between age-groups (Fig. 2; Table 2). Moreover, cytologic characteristics of ganglion cells including size and somatic staining were similar between age groups (Fig. 2). Irregularly shaped clusters of heterogeneous vesicles were observed with the transmission electron microscope in the IHC cytoplasm of older animals but other ultrastructural features including mitochondria appeared normal. By comparison, OHC loss was more advanced in older animals (Fig. 3). The organ of Corti of

Table 1
Subject age and function

	Age (weeks)	8 kHz ABR threshold (dB SPL)	16 kHz ABR threshold (dB SPL)	32 kHz ABR threshold (dB SPL)
Young group				
Y1	13	22.5	22.5	–
Y2	9	–	–	–
Y3	12	35.1	21	49.5
Old group				
O1	35	63.7	83.5	NR
O2	35	33.5	81	NR
O3	46	79.1	96.5	NR

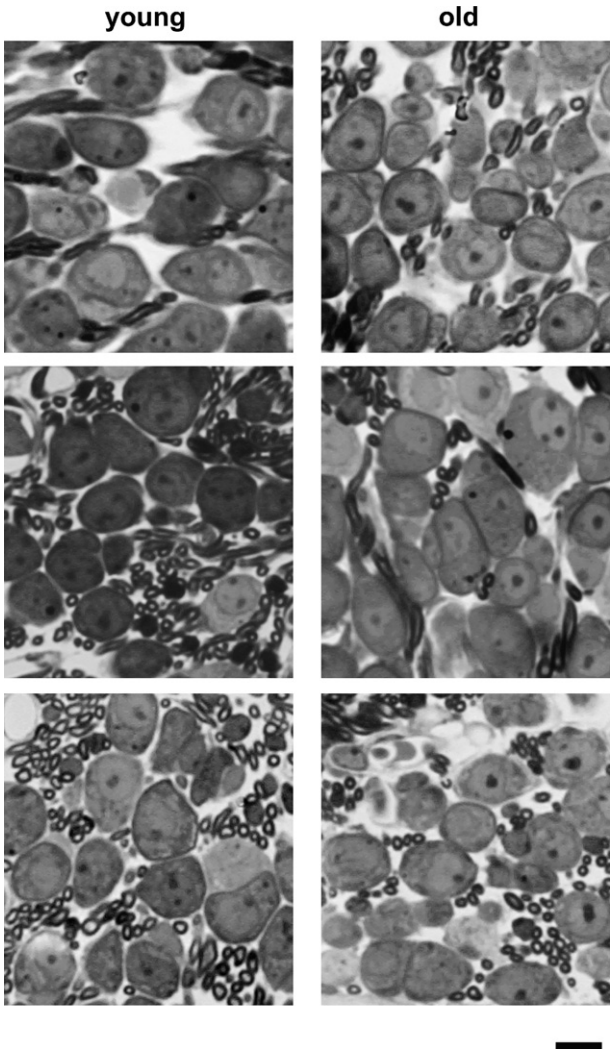

Fig. 2. Photomicrographs of the spiral ganglion region innervating IHCs under study. There was no difference in the cytology or density of SGCs in three older versus three younger animals (young and old mean densities (see Table 2): 3.073 ± 0.184 (10^{-3}) cells/μm^2 and 3.155 ± 0.121 (10^{-3}) cells/μm^2, respectively). Scale bar equals 20 μm.

Table 2
Histological characteristics of cochlear region under study

	Cochlear location studied (% re: base)	Number of IHCs examined	% OHC loss	IHC density (cells/mm)	SGC density (cells/μm^2)
Young group					
Y1	48	4	0	100	3.05×10^{-3}
Y2	40	4	0	127.9	2.83×10^{-3}
Y3	47	2	0	137	3.26×10^{-3}
Old group					
O1	47	3	70.1	97.3	3.02×10^{-3}
O2	45	3	40.5	102.2	3.22×10^{-3}
O3	47	3	100	81.6	3.23×10^{-3}

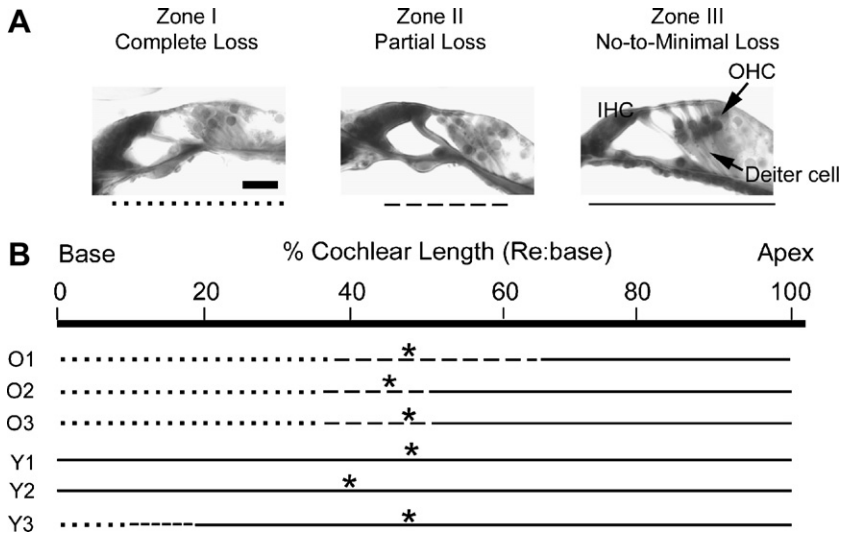

Fig. 3. (A) Three zones of OHC loss in older animals are illustrated by photomicrographs of the organ of Corti. There is a basal zone of complete OHC loss (Zone I), a transition zone of partial OHC loss (Zone II) and an apical zone of preserved OHCs (Zone III). The loss of OHCs is derived from decrements in the one-to-one relationship between Deiter cells and OHCs. (B) Cytocochleograms mapped the zones of complete OHC loss (dotted line), partial OHC loss (dashed line), and no loss of OHCs (solid line) for each cochlea studied. The sites of ultrastructural analysis, indicated by asterisks, are associated with partial OHC loss in older animals, but no loss in younger animals. Scale bar equals 20 μm.

these animals exhibited three relatively distinct regions. A basal region of essentially complete OHC loss (zone I) extended to the middle of the cochlea which was characterized as a transitional zone of partial loss (zone II). The remainder of the apical cochlea exhibited minimal or no cell loss (zone III). The cochlear region under study showed partial loss of its OHCs in older animals, but was cytologically normal in younger animals (Fig. 3).

3.1. Inner hair cells lose afferent contacts in older animals

Each radial fiber terminated at the inferior pole of a single IHC forming a single swelling that contained one afferent synaptic contact. This synapse was defined by a well-circumscribed area of apposing electron dense membranes, with the postsynaptic density (PSD) appearing more prominent. The density appeared as a fuzzy, filamentous matrix. In most cases, an electron-dense synaptic body (SB) was anchored to the presynaptic membrane where it was surrounded by a halo of round vesicles (Fig. 4). This synapse was an unambiguous marker for afferent radial fibers. Afferent fibers that did not contain a synapse rarely made contact with the IHC and were distinguishable from efferent axons when followed in serial section by the absence of homogenous clear vesicles at contacts with other dendrites or the IHC.

Despite comparable densities of spiral ganglion cells, there were fewer afferent synapses formed by radial fibers with IHCs in older compared to younger animals (Fig. 5). Younger animals exhibited on average 16.8 ± 2.4 (mean $\pm$ SD) synapses per IHC compared to 9.2 ± 3.1 in older animals (Mann–Whitney test, unpaired analysis, $Z = 3.55$, $p < 0.0005$). Variability within both age groups was noted.

There was non-uniform loss of afferent synapses around the circumference of the cylindrical IHC but uniform loss along the height of the IHC. The vertical distribution of afferent synapses (mean height of SB from inferior pole of IHC) was equivalent between older (4.1 ± 2.7 μm) and younger (3.9 ± 2.7 μm) animals. The radial distribution of these synapses, however, differed between age groups. Older animals exhibited a disproportionate loss of synapses on the surface of the IHC facing the cochlear base (the high frequency surface), and a relative preservation of synapses on the surface facing the cochlear apex (the low frequency surface). The reconstructed IHCs and afferent terminals, when viewed from the modiolus (Fig. 6A) or from below the IHC (Fig. 6C) demonstrate the homogenous radial distribution of terminals in younger animals and of the selective loss of terminals on the high frequency surface in older animals. The radial position of each synapse was measured as an angle relative to a reference line perpendicular to the pillar cells and passing through the center of the IHC (Fig. 6D). Synapses on the low-frequency surface of the IHC were assigned angles $0° < x < 180°$, whereas the remaining synapses were located on the high-frequency surface. The difference in distribution between high- and low-frequency surfaces of the IHC was statistically significant between age groups ($\chi^2 = 11.9$, $p < 0.001$; Fig. 6D). There was, however, no difference in the distribution of synapses along the pillar-modiolar dimension.

3.2. Terminal morphology is altered in older animals

Morphological measurements were made in 167 endings forming afferent synapses with 10 IHCs in young animals and 82 endings innervating 9 IHCs in old animals. Morphometric data were calculated from cross-sectional pro-

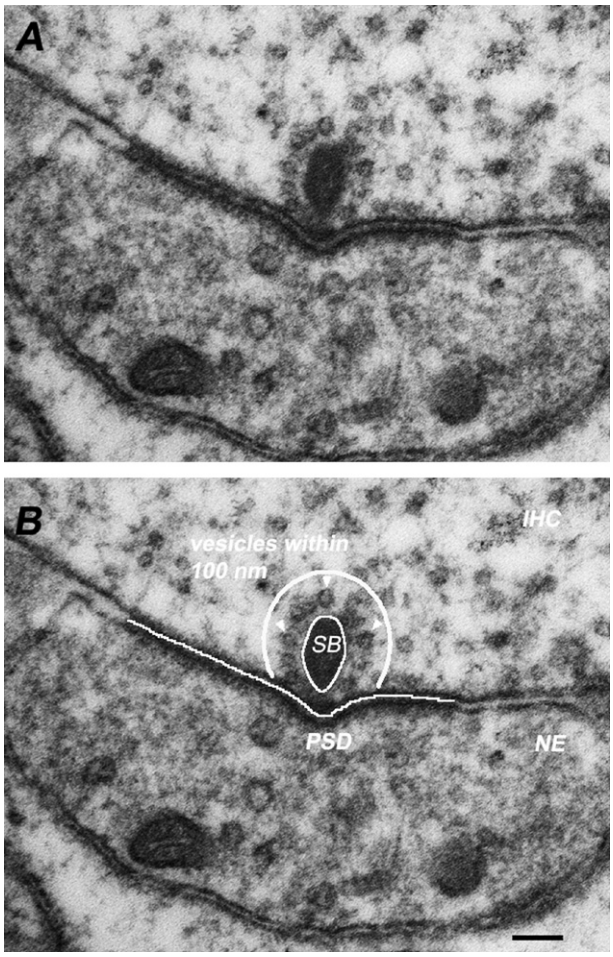

Fig. 4. Electron micrograph of synapse between IHC and afferent radial terminal (A) illustrating key features identifying afferent nerve terminals (B). The synaptic release site is characterized by closely apposed and asymmetrically thickened membranes of the IHC and afferent terminal. The postsynaptic density (PSD) is conspicuous by an accumulation of dense material on its cytoplasmic surface. This material appears as a granular bed with filamentous protrusions. PSDs are usually associated with an electron dense presynaptic ribbon or synaptic body (SB) that is surrounded by a halo of clear round vesicles (arrowheads). Vesicles located within 100-nm of the SB (indicated by solid line) and those docked at the pre-synaptic membrane were counted. Scale bar equals 100 nm.

files in semi-serial sections (Fig. 7A and B). Terminal and mitochondrial volumes were calculated as the product between profile areas and the interval distance between sections (Fig. 7C).

3.2.1. Afferent terminal size

As can be appreciated in 3D reconstructions in Fig. 6, afferent terminals were significantly larger in older compared to younger animals (Mann–Whitney, $Z = 8.2$, $p < 0.0001$) (Fig. 8A). Not surprisingly, a parallel increase in the apposition surface area between terminals and IHCs was also observed (Mann–Whitney, $Z = 7.33$, $p < 0.0001$, data not shown). Despite a reduction in the number of innervating terminals, the summed apposition area between terminals and IHCs was not significantly different

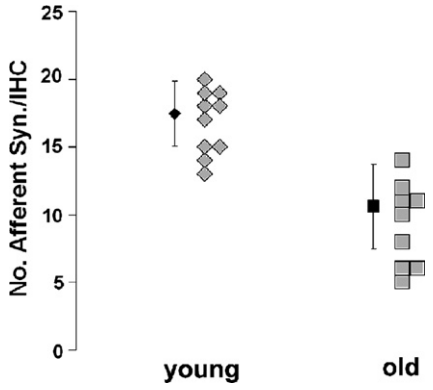

Fig. 5. Plot of the number of afferent terminals forming synapses with IHCs. Despite inter-animal variability in the innervation density between IHCs of the same age, there is a significant difference between young and old animals. (Mann–Whitney test, unpaired analysis, $Z = 3.55$, $p < 0.0005$). Afferent innervation loss of the inner hair cells is a major aging event in C57BL/6J mice.

for older animals ($47.5 \pm 24.9\ \mu m^2$/IHC) compared to younger animals ($32.2 \pm 6.3\ \mu m^2$/IHC; $t = 1.9$, $p > 0.05$). The aggregate area of the sensory–neural interface at individual IHCs is thus relatively preserved and in some cases expanded despite loss of afferent contacts.

There was no systematic relationship between terminal size and spatial location in young animals, but regional variations were observed in older animals. When normalized to the largest terminal volume innervating each IHC, older animals demonstrated the largest endings on the low-frequency surface facing the pillar cells (0–90°), and the smallest on the high-frequency surface facing the modiolus (180–270°). With respect to IHC quadrant, the difference in terminal size approached statistical significance (ANOVA $F = 2.46$, $p = 0.07$). Terminal size distribution is therefore consistent with the enlargement of some endings and possible loss of smaller ones located on the high frequency surface of the IHC.

3.2.2. Terminal mitochondrial content

The total mitochondrial volume contained within each terminal was estimated as the product of section interval thickness and the sum total of all mitochondrial profile areas (Fig. 7C). The mitochondrial volume within nerve endings in older animals ($0.49 \pm 0.0.52\ \mu m^3$) was significantly greater than that seen in younger animals ($0.15 \pm 0.13\ \mu m^3$; Mann–Whitney, $Z = 5.88$, $p < 0.0001$). These data confirm an average increase of mitochondrial content in the surviving terminals (Fig. 8B). There was also a proportional increase in mitochondrial volume with terminal size seen in both young ($r = 0.8$, $p < 0.0001$) and old ($r = 0.78$, $p < 0.0001$) mice.

Since the mean number of mitochondrial profiles per terminal profile was the same in younger (3.60 ± 3.45) and older animals (3.17 ± 2.00; Mann–Whitney, $Z = 0.3$, $p > 0.05$), the growth in mitochondrial content observed

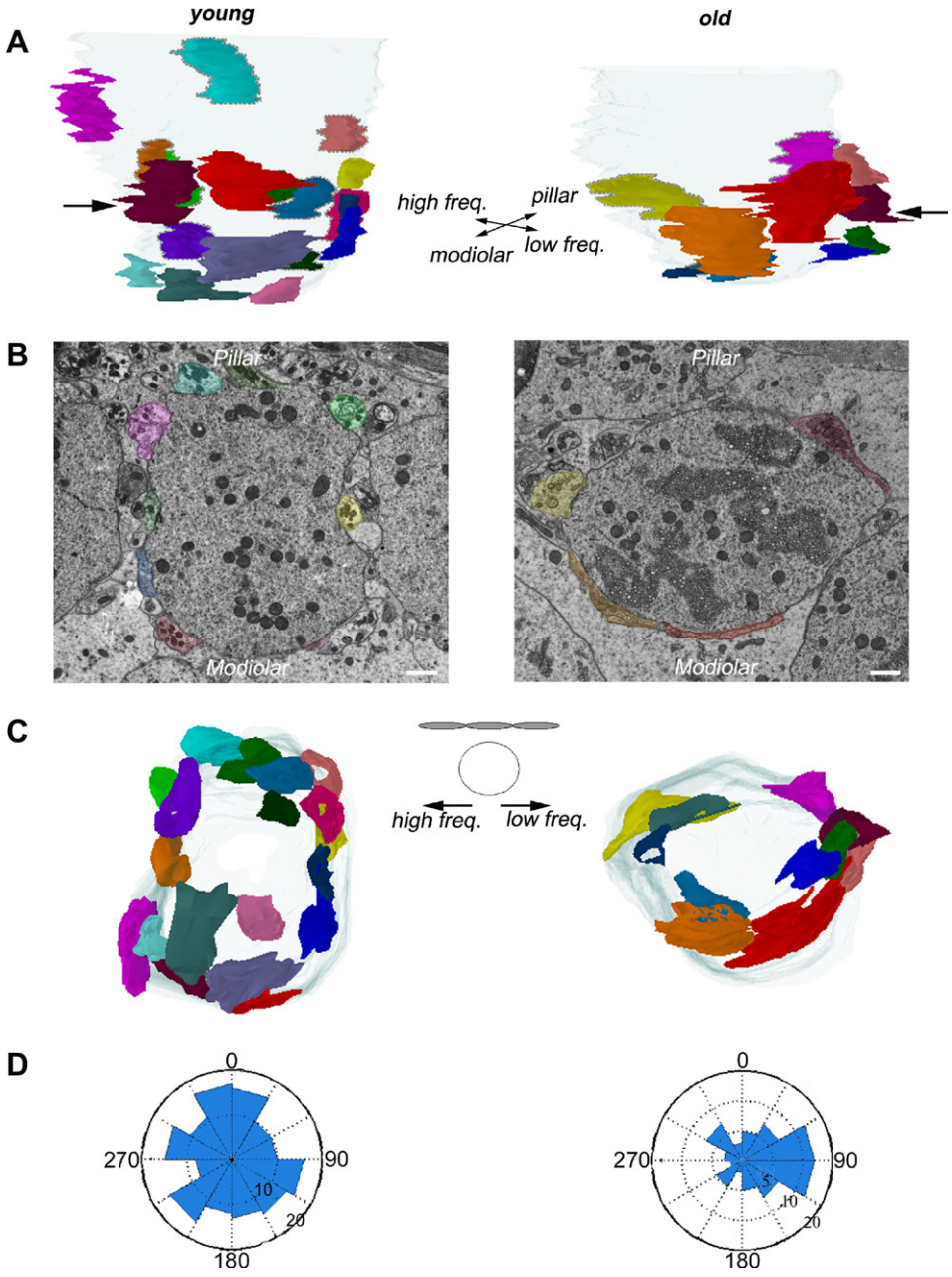

Fig. 6. There is an age-dependent change in the radial distribution of afferent terminals and their synapses with IHCs. (A) Three-dimensional reconstruction of IHCs viewed from the modiolus, show a reduction in the number of afferent terminals, an increase in their size and a tendency for them to populate the low-frequency surface in older compared to younger animals. Arrows indicate the approximate position of the electron micrographs shown below. (B) Transmission electron micrographs demonstrate typical differences in cross-sectional anatomy between older and younger age groups. (Scale bar 1 μm; also applies to reconstructions). (C) Inferior views of neural pole of same IHCs demonstrate the typical difference in the radial distribution of afferent terminals between age groups. In older animals, afferent terminals are more likely to be located on the low-frequency side of the hair cell compared to the high-frequency side. (D) "Rose" plots illustrate this distributional difference for all IHCs under study. Whereas significant differences in afferent synaptic distribution on the high- versus low-frequency surfaces of the IHC ($\chi^2 = 11.9$, $p < 0.001$) were observed between older and younger animals, there was no effect of age on pillar versus modiolar distribution. Terminal location appears to influence the loss or preservation of afferent innervation.

in older animals resulted from an increase in mitochondrial size. Electron micrographs of typical afferent terminals demonstrated larger mitochondria in older compared to younger animals with preservation of normal ultrastructure. The cross-sectional areas of individual mitochondrial profiles found within afferent terminals were measured in alternate sections. The mean cross-sectional area of individual mitochondria increased from $0.023 \pm 0.021\ \mu m^2$ in younger animals to $0.07 \pm 0.06\ \mu m^2$ in older animals (Mann–Whitney, $Z = 55.5$, $p < 0.0001$).

The relationship between auditory nerve fiber physiology, the number of mitochondrial profiles per terminal and terminal location in cat (Liberman, 1980b, 1982; Liberman et al., 1990) prompted a similar analysis of terminal

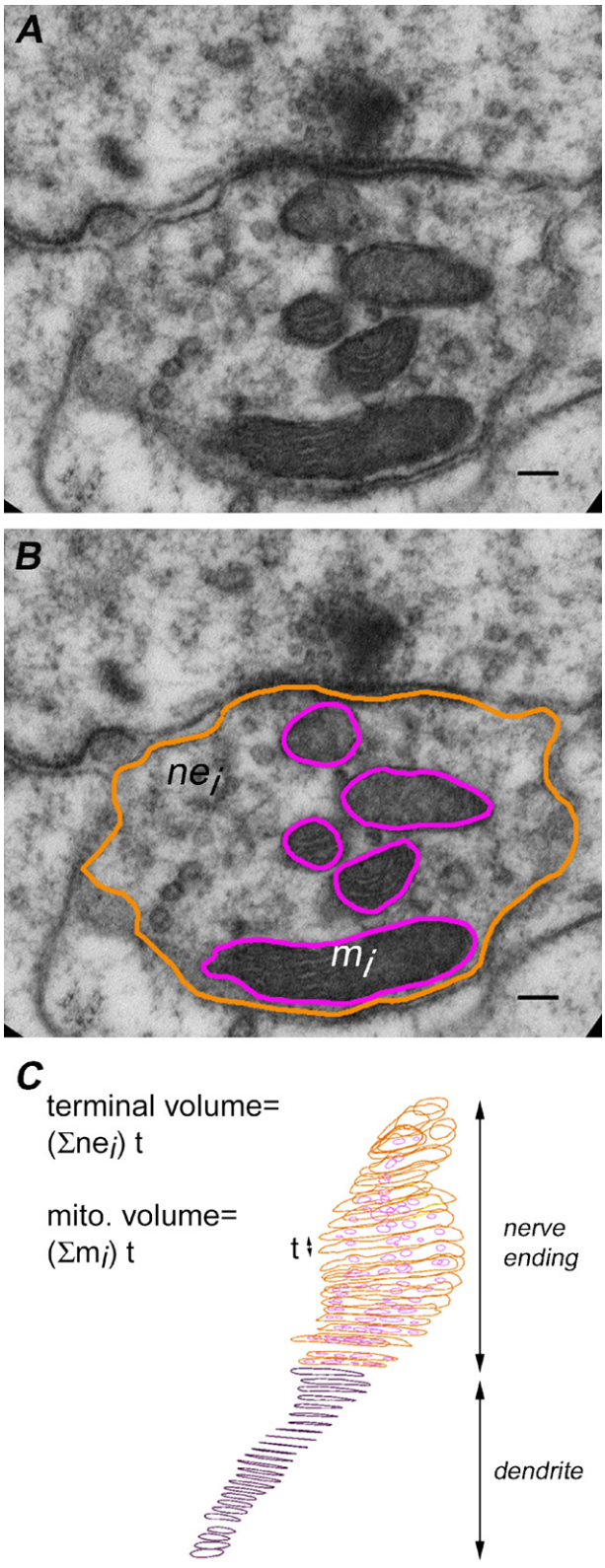

Fig. 7. Morphological measurements of the afferent terminal. (A) Electron micrograph showing the profile of an afferent terminal (ne_i) in the ith section. (B) The outer terminal membrane (orange line) and mitochondrial profiles (m_i) are traced in preparation for morphometric measurements. (C) When individual sections separated by distance t are stacked and aligned in 3D space, the resulting profiles permit the calculation of terminal volume and mitochondrial content. Scale bar equals 100 nm.

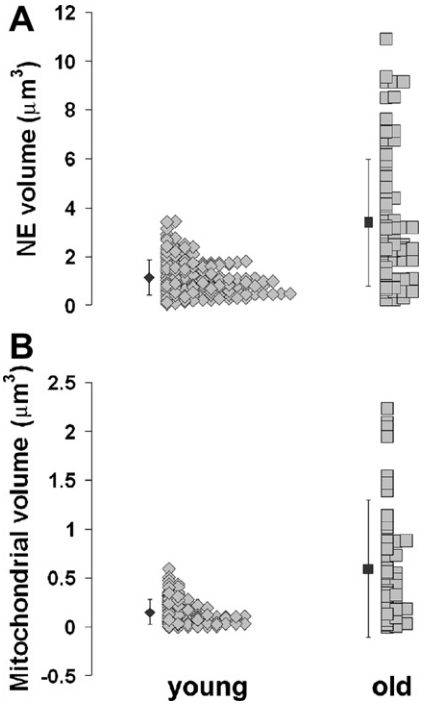

Fig. 8. Morphometric data from afferent terminals. (A) The mean volume of nerve endings is larger in older animals. The size distribution reveals growth of some terminals and a loss of smaller ones. (B) Terminal mitochondrial volume increases with age. Aging is associated with terminal and mitochondrial enlargement and the loss of smaller endings.

morphology and spatial distribution in mouse. In older but not younger C57BL/6J mice, mitochondrial content (average number of profiles per terminal profile) revealed significantly lower values on the modiolar surface of the IHC (2.60 ± 1.71) compared to the pillar surface (3.78 ± 2.13 ; Mann–Whitney, $Z = 2.71$, $p < 0.01$). In this mouse strain, mitochondrial volume did not reveal any spatial patterns.

3.3. Afferent synaptic morphology is altered in older animals

Older animals exhibited striking differences in synaptic morphology and size compared to younger animals. Moreover, the larger synaptic bodies in older animals were likely to have lucent cores and be associated with higher numbers of vesicles. PSDs in older animals also exhibited differences in cross-sectional shape and were associated with greater numbers of docked vesicles.

3.3.1. Synaptic body morphology

Whereas a PSD is typically associated with a single SB, older animals exhibited a higher prevalence of PSDs associated with multiple SBs or without any SBs. Younger animals exhibited nine isolated PSDs out of a total of 167 PSDs, whereas older animals featured 12 out of 82; moreover, older animals had a greater proportion of PSDs

associated with multiple SBs (10 of 167 young versus 18 of 82 old) ($\chi^2 = 22.4$, $p < 0.0001$).

Multiple SBs were preferentially found in older mice on the IHC surface with the greatest loss of afferent synapses. There was however, no difference in the radial distribution of synapses with multiple SBs in younger animals: 4 of 84 terminals on the high frequency surface of the IHC and 6 of 83 terminals on the low frequency surface ($\chi^2 = 0.5$, $p > 0.05$). Older animals exhibited a higher incidence of multiple SBs on the high frequency surface (9 of 22 terminals) compared to the low frequency surface (9 of 60 terminals) ($\chi^2 = 5.7$, $p < 0.05$). There was no significant difference in the spatial distribution of PSDs without SBs.

Synaptic bodies were larger in older animals (Fig. 9). Representative examples of synaptic bodies from young and old animals are presented in semi-serial section to the mid-section, demonstrating the marked difference in SB size and morphology between these age groups (Fig. 9). Older SBs were larger both in cross-sectional area and length. Synaptic body surface area was estimated from alternate serial sections as:

$$\text{SB surface area} = \sum p_i t,$$

where p_i is the SB perimeter (Fig. 4) and t is the interval distance between sections. Synaptic body surface area increased from $0.05 \pm 0.02\ \mu m^2$ in younger animals to $0.11 \pm 0.06\ \mu m^2$ in older animals (Fig. 9B, $t = 12.44$, $p < 0.0001$). A cumulative probability plot demonstrated a greater likelihood that older animals possess larger SBs than younger animals (Fig. 9C). Synaptic bodies with a central lucency were more common in older mice (26 of 71 SBs) as compared to younger ones (33 of 164 SBs; $\chi^2 = 7.17$, $p < 0.01$).

Although synaptic body shape was, on average, the same between young and old animals, spatial distribution by shape differed between the age groups. Aspect ratio was used as a measure of SB shape and was calculated as the ratio of largest to smallest dimensions of each profile averaged across alternate sections. In young animals, SBs on the modiolar surface were more likely to be columnar (aspect ratio $= 2.24 \pm 0.70$), whereas those on the pillar surface were more likely to be oval (aspect ratio $= 1.77 \pm 0.44$; $t = 5.1$, $p < 0.0001$). In older animals, however, there was no spatial variation in SB shape, and the mean aspect ratios on pillar and modiolar sides were 1.97 ± 0.53 and 2.01 ± 0.63, respectively.

3.3.2. Postsynaptic density morphology

The PSD of the afferent fiber did not differ in thickness between age-groups, but there was a change in shape. The thickness of the PSD measured between the cytoplasmic junction of IHC and terminal membranes was the same for both the most degenerated cochlea in the older group (62.0 ± 13.2 nm) and a normal cochlea from the younger group (61.8 ± 29.6 nm). A linear central indentation of the PSD oriented parallel to the long axis of the IHC was observed in cross-sections. The indentation was deepest where the SB was in closest contact (Fig. 10). Postsynaptic

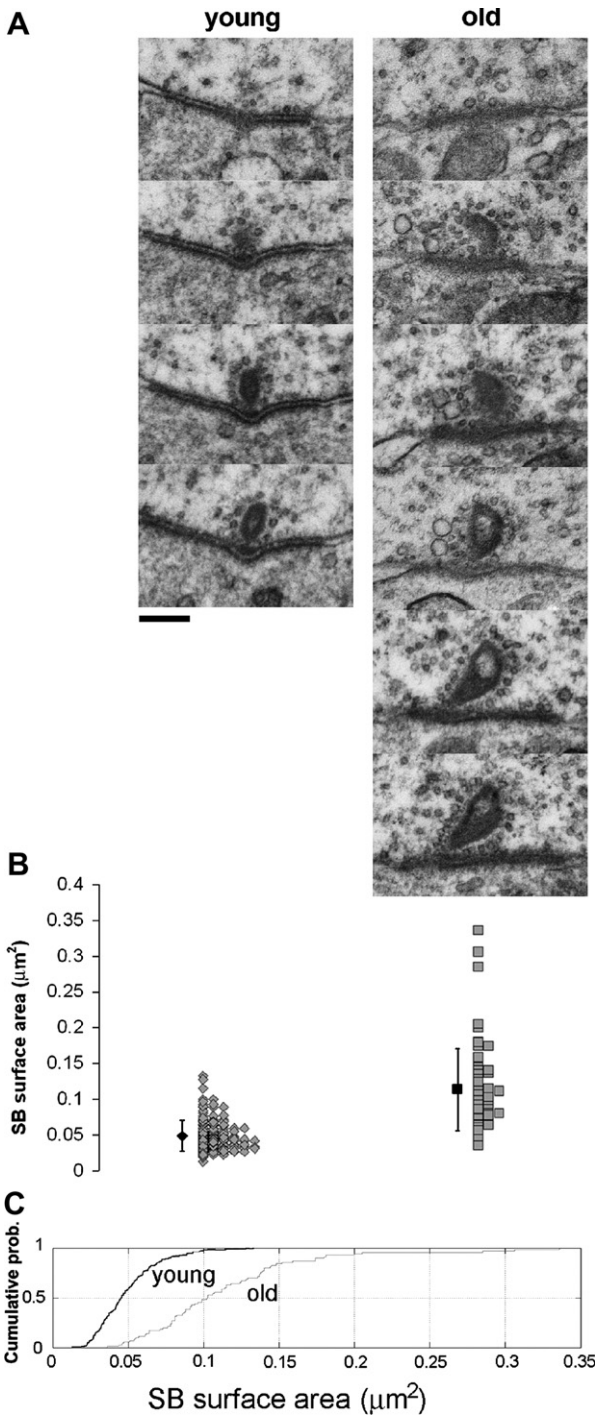

Fig. 9. Comparison of SB morphometry between young and old animals. (A) Serial section electron micrographs illustrate larger SBs, larger numbers of vesicles associated with the SB, and a flattening of the PSD in older compared to younger animals. Scale bar equals 200 nm. (B) A plot of the reconstructed surface area of SBs shows that they are larger in older than younger animals. (C) Cumulative probability plot shows that half the SBs in older animals are larger than the largest SB in younger animals. Changes in SB size and associated vesicle number undoubtedly influence synaptic transmitter release and nerve ending firing properties.

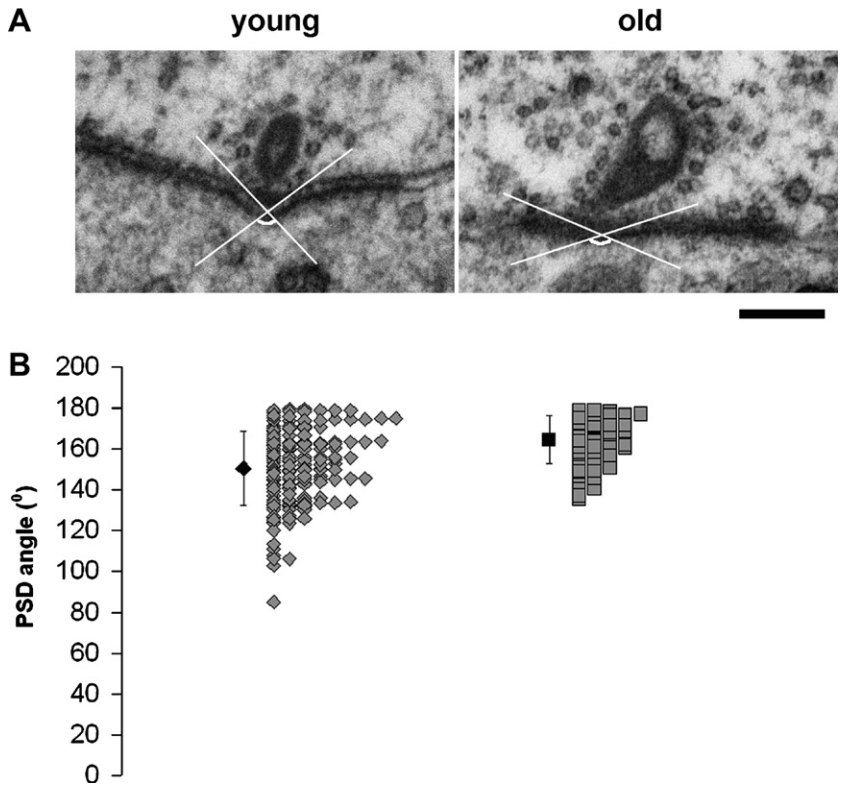

Fig. 10. Age-related changes to the angle of central PSD indentation. (A) The angle of indentation of the PSD at the mid-section through the SB was measured as shown in these representative examples from young and old mice. The PSD indentation is more acutely angled in the younger animal, whereas it is "flattened" in the older animal. (B) A plot of group data from young and old animals confirms this general feature and reveals a greater variability in angles among the younger animals. Scale bar equals 200 nm.

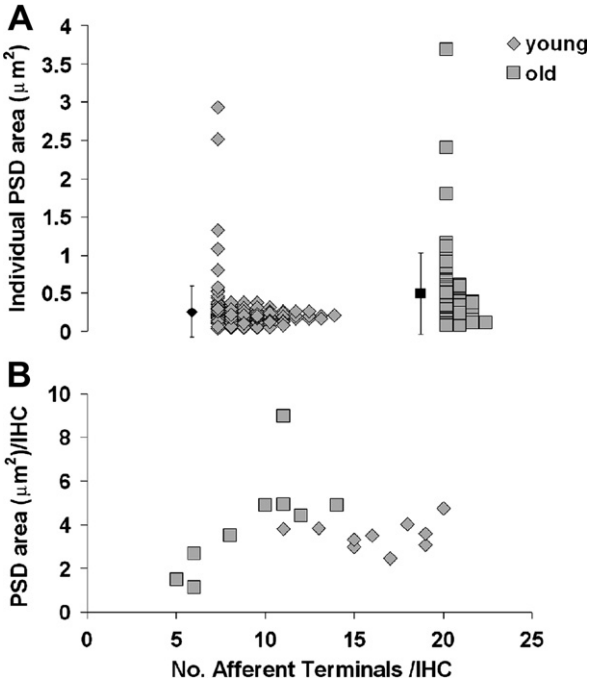

Fig. 11. Age-related changes to PSD features. (A) The mean area of reconstructed PSDs is larger in older animals due both to the loss of smaller synapses and the enlargement of remaining synapses. (B) A reduction in number of synapses is accompanied by an increase in PSD area which seems to preserve the aggregate PSD area per IHC. This compensatory response is not sufficient to maintain PSD area, however, when the number of endings falls below 10.

densities with the most acutely angled indentations were preferentially found in younger animals, whereas those in older animals were likely to be less angled and flatter in appearance (Mann–Whitney, Z-value $= 4.82$, $p < 0.0001$).

The area of the PSD was on average larger in older ($0.49 \pm 0.53\ \mu m^2$) compared to younger animals ($0.23 \pm 0.19\ \mu m^2$; Mann–Whitney, $Z = 6.2$, $p < 0.0001$, Fig. 11A). Despite variability in the number of PSDs per IHC and a reduction in older animals, the summed area of associated PSDs was relatively constant across IHCs (Fig. 11B). The total PSD area per IHC averaged $3.5 \pm 0.6\ \mu m^2$ in older mice compared to $4.1 \pm 2.4\ \mu m^2$ in younger mice ($t = 0.74$, $p > 0.05$). There was no variation in PSD size as a function of radial position on the IHC surface.

3.3.3. Vesicle density

Synapses were randomly selected to count vesicles associated with the SB and PSD. The criterion for selection was the presence of distinct membranes of the IHC and nerve terminal at synaptic sites. Consequently, analysis was restricted to the lateral surface of IHCs and not at the inferior pole which tended to curve within the section thickness and create blurring of membranes. A homogenous population of round vesicles measuring 28.96 ± 0.41 nm in diameter was closely associated with the SB and PSD. The number of vesicles in the central section through

the SB was counted within a radius of 30 and 100 nm of the SB margin (Fig. 4). The number of vesicles making contact with the presynaptic membrane at the PSD was also counted and these vesicles were referred to as "docked".

The number of clear vesicles observed within 30 nm of the SBs in older animals (15.8 ± 5.3) was greater compared to that of younger ones (10.4 ± 3.5; $t = 4.6$, $p < 0.0001$; Fig. 12). A similar trend was observed within 100 nm of the SB (29 ± 8.5 versus 18.3 ± 4.4, $t = 6.3$, $p < 0.0001$). As the surface area of the SB (perimeter × section thickness) under examination increased, so did the number of associated vesicles (Fig. 12A). This correlation was significant in both young ($r = 0.48$, $t = 3.5$, $p < 0.005$) and old animals ($r = 0.6$, $t = 2.82$, $p < 0.05$). Vesicle density relative to the SB surface was represented by the slope of the relationship (Fig. 12A), which was similar for young and old animals. Growth of synaptic body size was therefore associated with a proportional increase in the number of vesicles in the immediate vicinity of the synapse. An increase in the number of docked vesicles in older animals (5.9 ± 3.2 versus 3.7 ± 1.9, $t = 3.2$, $p < 0.005$) was associated with an increase in PSD area (Fig. 12B).

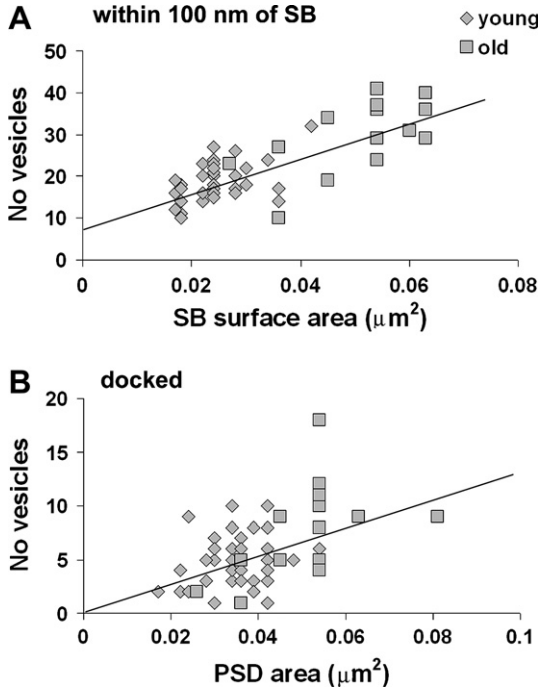

Fig. 12. Age-related changes in synaptic vesicle characteristics. An increase in the population of synaptic vesicles accompanies the growth of the SB and PSD. The number of vesicles was counted in the mid-section through the SB (see Fig. 4) and was compared to the surface areas of the SB and PSD in the corresponding section (profile length × section thickness). (A) The increase in number of vesicles counted within 100 nm of the SB in older animals is proportional to enlargement of SB surface area ($r = 0.77$, $p < 0.0001$). (B) A positive correlation is seen between the number of docked vesicles making contact with the presynaptic membrane and the surface area of the PSD ($r = 0.48$, $p < 0.0001$). The increased population of vesicles appears driven by enlargement of SBs and PSDs, and may be a compensatory mechanism of a less efficient old synapse.

4. Discussion

We describe age-related structural changes at the synaptic interface between afferent nerve endings and IHCs in C57BL/6J mouse, an animal model of presbycusis. The number of radial fiber afferent synapses is reduced in excess of spiral ganglion cell loss and precedes IHC loss. Structural changes below the resolution of the light microscope are likely to accompany even earlier stages of hearing loss than were examined here. A report of lower distal and higher proximal fiber densities in the basal osseous spiral lamina of aging C57BL/6J mice (White et al., 2000) is consistent with our observation regarding age effects on synaptic contact and cell body densities. A subset of aged humans with down-sloping hearing loss exhibits minimal hair cell and spiral ganglion cell loss, but a deficit of radial fibers in the osseous spiral lamina (Nadol, 1979; Pauler et al., 1986; Spoendlin and Schrott, 1988, 1990; Chen et al., 2006). Collectively, these findings imply that afferent pathology starts in the most peripheral processes of the spiral ganglion cell, possibly at the synapse, and progress toward the cell body. The progression is consistent with the concept of 'dying back' (Cavanagh, 1964). What, however, are the biological mechanisms that determine preservation of synaptic contacts with IHCs? Degenerative and trophic processes at the auditory nerve-IHC interface may determine the ultimate fate of this synapse and provide future therapeutic options.

4.1. Afferent terminal fate in aging

Why terminals fail to maintain contact with IHCs is not known but their location and size appear to be predictive factors. The disproportionate loss of afferent innervation from the high-frequency side of IHCs (Fig. 6) implies regional differences in susceptibility to injury or efficacy of repair. Regional differences in the reaction by terminals to stressors such as glutamate excitotoxicity may explain the higher propensity for smaller endings on the high-frequency surface of the IHC to be lost, while larger terminals on the low-frequency surface are spared. Variability in the protection of terminals by supporting cells may also play a role. Differences in the spatial expression of GLAST by supporting cells have been reported around the IHC (Furness and Lawton, 2003), possibly rendering some terminals more susceptible to glutamate-induced excitotoxicity than others. Supporting cells also participate in signaling pathways that promote spiral ganglion cell survival by producing erbB4, which activates neuregulins generated by the spiral ganglion (Stankovic et al., 2004). Support of spiral ganglion cell survival by the β2 subunit of the nicotinic acetylcholine receptor (Bao et al., 2005) implies the role of lateral olivocochlear efferents in the maintenance of IHC innervation. Spatial differences in the density of axodendritic contacts by these efferents in mouse, if similar to observations in cat (Liberman, 1980b; Liberman et al., 1990), may contribute to the non-uniform loss of synapses

in aging animals. Such differences in the trophic effects of supporting cells and lateral olivocochlear efferents may therefore influence afferent innervation and structure.

There may also be differences among terminals in their intrinsic protective mechanisms. The ''folded'' morphology previously characterized in C57BL/6J mice may influence a terminal's destiny (Francis et al., 2004). The folded ending was observed mostly in 3-month-old mice exhibiting early cochlear dysfunction and hair cell loss. The folded morphology may indicate an intermediate phase in the response by afferent terminals to sensory pathology or metabolic stresses such as excessive glutamate exposure. If the folded morphology is a precursor to terminal enlargement through an ''unfolding'' step, it may explain the prevalence of large endings and rarity of folded endings (4 out of 82) in older mice. Terminals that are unable to acquire and maintain this folded morphology may be lost. Although the physiological relevance of terminal size in this context is unclear, the accommodation of mitochondrial growth to meet growing metabolic needs of the terminal is a possible explanation.

4.2. Aging morphology at the afferent synapse

The increased incidence of morphological features in older mice that are also seen in neonatal mice may reflect regenerative processes in surviving afferent contacts. Synapses with multiple SBs, a flattening of the PSD, and a loss of PSD concave indentation as observed in older animals represent a recapitulation of normal development (Sobkowicz et al., 1982). Synapse turnover in older animals is suggested by the absence of SBs at 22% of the PSDs and a larger incidence of multiple SBs. The increased incidence of synapses with multiple SBs is also observed in the mouse retina following partial photoreceptor loss (Jansen et al., 1997), suggestive of a reactive response to neural damage. These predominantly pre-synaptic changes could conceivably be induced within the cell by changes in vesicle recycling or extrinsically by efferent input to the IHC. Alternatively, they may be induced by on-going changes in IHC physiology as the organ of Corti ages.

Afferent loss, synapse turn-over and morphological changes at the neural pole of the IHC may be the manifestations of a defective mechanoelectrical transduction apparatus at the apical pole of the cell. Abnormal tip link structure in hair cell stereocilia resulting from a cadherin 23 mutation in C57BL/6J mice (Noben-Trauth et al., 2003; Siemens et al., 2004) is associated with increased susceptibility to noise overexposure and age-related hearing loss in several mouse strains. The progression of functional deficits implies accumulative pathology that may be mediated by pre- and postsynaptic responses to abnormal stereocilia transduction. In the absence of normal tip link organization and relationships (Di Palma et al., 2001), sound-induced changes in IHC membrane potential may be more erratic than normal. As a result, large fluctuations could occur in the amount of glutamate released resulting membrane potential responses to sound may become erratic producing large fluctuations in glutamate release that induce episodic excitotoxic injury at afferent synapses. The accumulation of these injuries over time may alter terminal structure and hearing function.

Terminal enlargement may be an example of the accumulative effects of chronic excitotoxic injury, representing direct pathology, adaptive responses to injury, or both. The repeated occurrence of transient acute enlargement of terminals in response to excess glutamate release (Puel et al., 1998) may lead to irreversible changes in terminal morphology that ultimately lead to denervation. Alternatively, changes in terminal morphology may represent the normal adaptive response by radial dendrites against the threat of glutamate excitotoxicity. Dendritic spine shape in the CNS, for example, is influenced by glutamate concentration (Halpain et al., 1998, 2005), including ''spine collapse'', which is an early observation in several chronic neurodegenerative diseases linked to excitotoxic injury. A variety of alterations of dendrite morphology including swelling is also reported in the aging CNS (Lolova et al., 1997). Glutamate-induced changes in spine shape appear to be mediated by F-actin associated enzyme pathways that alter both the cytoskeleton and microenvironment of the spine (Halpain et al., 1998, 2005). For neurons that survive glutamate overexposure, the associated depolymerization of F-actin is excitoprotective against subsequent glutamate exposures through the blunting of calcium influx (Furukawa et al., 1995). The relevance of these observations in the CNS to radial dendrites in the cochlea is unknown, but they are consistent with the notion that accumulative effects of glutamate excitotoxicity on the terminal cytoskeleton may lead to bouton enlargement while also providing a survival advantage to these terminals. This idea is further supported by the presence of smaller terminals on the high-frequency surface of the IHC, with the least number of remaining endings, compared to the relatively better preserved larger endings on the low-frequency surface.

4.3. The morphology of synaptic compensation

As demonstrated in the CNS, synapses also undergo adaptations to optimize information transfer within the auditory pathway. Alterations in the size and shape of synaptic specializations in the developing (Taschenberger et al., 2002) and mature brain (Geinisman et al., 1996) are associated with changes in synaptic efficacy (Lisman and Harris, 1993) and offer some insights into compensatory synaptic mechanisms that may be relevant in the auditory periphery. Activity-related mechanisms at IHC synapses may produce changes in response to diminished sensory transduction, reduced afferent innervation density or both. The inverse relationship between PSD area and the number of afferent contacts is an example of how morphological change may compensate for declines in afferent density. Indeed the proportional increase of the vesicle population relative to the enlargement of SB and PSD size

(Fig. 12A) suggests an underlying physiological impetus to maintain an optimal level of neural activity.

Ultrastructural responses to changes in pre-synaptic activity has been demonstrated in the auditory CNS and retina. Terminal and synaptic structure in the anterior ventral cochlear nucleus (AVCN) appear dependent on activity in the auditory periphery. The shape of endbulbs of Held and their synapses are modified by deafness in cats (Ryugo et al., 1997) and mice (Limb and Ryugo, 2000). Normal synaptic phenotype is restored, however, in endbulbs of young congenitally deaf cats after chronic stimulation of the auditory nerve with a cochlear prosthesis (Ryugo et al., 2005). In a similar fashion, light-induced changes in SB size and shape have been reported in mouse retina (Spiwoks-Becker et al., 2004). Larger and more elongated SBs are seen during exposure to the dark and are restored to smaller sizes in light.

4.4. Functional implications of aging morphology

Because the area of synaptic specialization is proportional to the probability of vesicular release, excitatory synapses that enlarge might also grow stronger (Murthy et al., 2001). Cochlear degeneration and the accompanying loss of hearing sensitivity could trigger compensatory mechanisms that attempt to preserve activity within the auditory pathway. Total PSD areas, for example, were remarkably preserved in several IHCs despite significant reductions in afferent input. The ''strengthening'' of synapses, however, may also be associated with faulty clearance of neurotransmitter (Walmsley et al., 1998), leading to prolonged postsynaptic currents and slower recovery from previous stimulation. Furthermore, as mitochondria increase in size, they become less efficient (Kowald and Kirkwood, 2000), implying that they are less able to provide energy for sustained activity. Slowed synaptic responses would desynchronize neural activity and have a negative impact on speech discrimination.

The functional relevance of afferent terminal and synapse structure has been demonstrated at IHCs in normal hearing cat (Liberman, 1980a). Terminal size, mitochondrial content, and synaptic morphometry are correlated with discharge properties of the corresponding auditory nerve fibers. The applicability of these observations to C57BL/6J mice and their relevance to the diseased cochlea are, however, unknown. These structure-function relationships are unlikely to be static and may vary with strain, age of the animal, activity, and disease. Computer models suggest that changes in multiple components of synaptic transmission, which may accompany ultrastructural changes such as those observed in this study, are likely to affect auditory nerve response properties (Krishna, 2002).

The appearance of spatially distinct terminal morphology in older animals coincides with the loss of spatially distinct SB morphology seen in younger animals. There was no clear segregation of terminals between pillar and modiolar surfaces in young animals based on size or mitochondrial content as observed in cats. However, there was a strong tendency for round SBs to occur on the pillar surface and columnar SBs to occur on the modiolar surface. In cats, spherical SBs were associated with high-SR fibers, whereas elongated SBs were associated with low SR fibers. Older animals, by comparison, demonstrated significantly more mitochondrial profiles in terminals on the pillar compared to modiolar surfaces, similar to findings in normal hearing cats and corresponding to high- and low-SR fibers respectively (Liberman, 1980a). This relationship could be related to fiber SR in the mouse. Moreover, the multifaceted nature of age-related changes in terminals and synapses emerge.

Large increases in terminal and mitochondrial size suggests that high-SR properties become more prominent. The greater prevalence of high-SR fibers at high frequencies in both C57BL/6J and CBA/CaJ mice (Taberner and Liberman, 2005) may provide a window into aging effects in the ''older'' portions of the basal cochlea, which is consistent with trends in terminal morphology seen in older animals. Such a change in SR distribution would also be consistent with the decline of low spontaneous rate fibers in aging animals (Schmiedt et al., 1996). The result would be a loss of fibers with larger dynamic ranges, strong responses to signals in noise, and the ability to phace lock and amplitude modulate (Joris et al., 1994). Such changes in auditory nerve composition may therefore be responsible for the disturbance of hearing in background noise demonstrated by C57BL/6J mice early in the progression of age-related hearing dysfunction (Prosen et al., 2003). If these relationships are also applicable to humans, they may help explain the poor speech discrimination of patients with presbycusis, particularly in background noise.

In conclusion, we report on structural features that may represent the early stages of a progression of age related hearing loss. The inability to detect these morphological changes at the light microscopic level may explain the imperfect correlation between hearing deficits and temporal bone findings (Schuknecht, 1994). The poor correlation between cochlear and central auditory degeneration in aging C57BL/6J mice (Willott and Bross, 1990, 1996) may also be explained by downstream effects of pathology at the first auditory synapse. It therefore appears that the presence or absence of hair cells and/or ganglion cells is not the crucial variable, and that more detailed physiological and anatomical data at the levels of the afferent terminal and synapse will be required to resolve the variables of auditory physiology, its dysfunction in disease and mitigation with therapy.

Acknowledgements

This research was supported by NIH/NIDCD Grants DC00143, DC05909, DC05211, DC00232, and by Grants provided by the American Hearing Research Foundation, Deafness Research Foundation and National Organization

for Hearing Research. We thank Elliot Hogg and Zeyar Min for their technical assistance.

References

Bao, J., Lei, D., Yafei, D., Ohlemiller, K.K., Beaudet, A.L., Role, L.W., 2005. Requirement of nicotinic acetylcholine receptor subunit β2 in the maintenance of spiral ganglion neurons during aging. J. Neurosci. 25, 3041–3045.

Bertoni-Freddari, C., Fattoretti, P., 1989. Computer-assisted morphometry of synaptic plasticity during aging and dementia. Pathol. Res. Pract. 185, 799–802.

Bertoni-Freddari, C., Fattoretti, P., Paoloni, R., Caselli, U., Galeazzi, L., Meier-Ruge, W., 1996. Synaptic structural dynamics and aging. Gerontology 42, 170–180.

Cavanagh, J.B., 1964. The significance of the "dying back process in experimental and human neurological disease. Int. Rev. Exp. Pathol. 3, 219–267.

Chen, M.A., Webster, P., Yang, E., Linthicum, F.H., 2006. Presbycusic neuritic degeneration within the osseous spiral lamina. Otol. Neurotol. 27, 316–322.

De Groot, D.M.G., 1988. Comparison of methods for estimation of the thickness of ultrathin tissue sections. J. Microsc. 151, 23–42.

Di Palma, F., Holme, R.H., Bryda, E.C., Belyantseva, I.A., Pellegrino, R., Kachar, B., Steel, K.P., Noben-Trauth, K., 2001. Mutations in Cdh23, encoding a new type of cadherin, cause stereocilia disorganization in waltzer, the mouse model for Usher syndrome type 1D. Nat. Genet. 27, 103–107.

Falia, J.C., Harris, K.M., 2001a. Extending unbiased stereology of brain ultrastructure to three-dimensional volumes. J. Am. Med. Inform. Assoc. 8, 1–16.

Falia, J.C., Harris, K.M., 2001b. Cylindrical diameters method for calibrating section thickness in serial electron microscopy. J. Microsc. 202, 468–472.

Francis, H.W., Ryugo, D.K., Gorelikow, M.J., Prosen, C.A., May, B.J., 2003. The functional age of hearing loss in a mouse model of presbycusis. II. Neuroanatomical correlates. Hear. Res. 183, 29–36.

Francis, H.W., Rivas, A., Lehar, M., Ryugo, D.K., 2004. Two types of afferent terminals innervate cochlear inner hair cells in C57BL/6J Mice. Brain Res. 1016, 182–194.

Francis, H.W., Rivas, A., Lehar, M., Saito, Y., Mouton, P.R., Ryugo, D.K., 2006. Efficient quantification of afferent cochlear ultrastructure using design-based stereology. J. Neurosci. Meth. 150, 150–158.

Furness, D.N., Lawton, D.M., 2003. Comparative distribution of glutamate transporters and receptors in relation to afferent innervation density in the mammalian cochlea. J. Neurosci. 23, 11296–11304.

Furukawa, K., Smith-Swintosky, V.L., Mattson, M.P., 1995. Evidence that actin depolymerization protects hippocampal neurons against excitotoxicity by stabilizing $[Ca^{2+}]_i$. Exp. Neurol. 133, 153–163.

Geinisman, Y., Detoledo-Morrell, L., Morrell, F., Persina, I.S., Beatty, M.A., 1996. Synapse restructuring associated with the maintenance phase of hippocampal long-term potentiation. J. Comp. Neurol. 368, 413–423.

Halpain, S., Hipolito, A., Saffer, L., 1998. Regulation of F-actin stability in dendritic spines by glutamate receptors and calcineurin. J. Neurosci. 18, 9835–9844.

Halpain, S., Spencer, K., Graber, S., 2005. Dynamics and pathology of dendritic spines. Prog. Brain Res. 147, 29–37.

Henry, K.R., Chole, R.A., 1980. Genotypic differences in behavioral, physiological and anatomical expressions of age-related hearing loss in the laboratory mouse. Audiology 19, 369–383.

Hequembourg, S., Liberman, M.C., 2001. Spiral ligament pathology: a major aspect of age-related cochlear degeneration in C57BL/6 mice. J. Assoc. Res. Otolaryngol. 2, 118–129.

Jansen, H.G., Hawkins, R.K., Sanyal, S., 1997. Synaptic growth in the rod terminals of mice after partial photoreceptor cell loss: A three-dimensional ultrastructural study. Microsc. Res. Tech. 36, 96–105.

Joris, P.X., Carney, L.H., Smith, P.H., Yin, T.C., 1994. Enhancement of neural synchronization in the anteroventral cochlear nucleus. I. Responses to tones at the characteristic frequency. J. Neurophysiol. 71, 1022–1036.

Kowald, A., Kirkwood, T.B., 2000. Accumulation of defective mitochondria through delayed degradation of damaged organelles and its possible role in the ageing of post-mitotic and dividing cells. J. Theor. Biol. 202, 145–160.

Krishna, B.S., 2002. A unified mechanism for spontaneous-rate and first-spike timing in the auditory nerve. J. Comput. Neurosci. 13, 71–91.

Li, H.-S., Borg, E., 1991. Age-related loss of auditory sensitivity in two mouse genotypes. Acta Otolaryngol. (Stockh) 111, 827–834.

Liberman, M.C., 1980a. Morphological differences among radial afferent fibers in the cat cochlea: an electron-microscopic study of serial sections. Hear. Res. 3, 45–63.

Liberman, M.C., 1980b. Efferent synapses in the inner hair cell area of the cat cochlea: an electron microscopic study of serial sections. Hear. Res. 3, 189–204.

Liberman, M.C., 1982. Single-neuron labeling in the cat auditory nerve. Science 216, 1239–1241.

Liberman, M.C., Dodds, L.W., 1984. Single-neuron labeling and chronic cochlear pathology. II. Stereocilia damage and alterations of spontaneous discharge rates. Hear. Res. 16, 43–53.

Liberman, M.C., Dodds, L.W., Pierce, S., 1990. Afferent and efferent innervation of the cat cochlea: quantitative analysis with light and electron microscopy. J. Comp. Neurol. 301, 443–460.

Limb, C.J., Ryugo, D.K., 2000. Development of primary axosomatic endings in the anteroventral cochlear nucleus of mice. J. Assoc. Res. Otolaryngol. 1, 103–119.

Lisman, J.E., Harris, K.M., 1993. Quantal analysis and synaptic anatomy – integrating two views of hippocampal plasticity. TINS 16, 141–147.

Lolova, I.S., Lolov, S.R., Itzev, D.E., 1997. Aging and the dendritic morphology of the rat laterodorsal and pedunculopontine tegmental nuclei. Mech. Ageing Dev. 97, 193–205.

Muller, M., von Huenerbein, K., Hoidis, S., Smolders, J.W., 2005. A physiological place-frequency map of the cochlea in the CBA/J mouse. Hear. Res. 202, 63–73.

Murthy, V.N., Schikorski, T., Stevens, C.F., Zhu, Y., 2001. Inactivity produces increases in neurotransmitter release and synapse size. Neuron 32, 673–682.

Nadol, J.B., 1979. Electron microscopic findings in presbycusic degeneration of the basal turn of the human cochlea. Otolaryngol. Head Neck Surg. 87, 818–836.

Noben-Trauth, K., Zheng, Q.Y., Johnson, K.R., 2003. Association of cadherin 23 with polygenic inheritance and genetic modification of sensorineural hearing loss. Nat. Genet. 35, 21–23.

Pauler, M., Schuknecht, H.F., Thornton, A.R., 1986. Correlative studies of cochlear neuronal loss with speech discrimination and pure-tone thresholds. Arch. Otorhinolaryngol. 243, 200–206.

Prosen, C.A., Dore, D.J., May, B.J., 2003. The functional age of hearing loss in a mouse model of presbycusis. I. Behavioral assessments. Hear. Res. 183, 44–56.

Puel, J.-L., Ruel, J., Gervais d'Aldain, C., Pujol, R., 1998. Excitotoxicity and repair of cochlear synapses after noise-trauma induced hearing loss. NeuroReport 9, 2109–2114.

Rivas, A., Francis, H.W., 2005. Inner ear abnormalities in a KCNQ1 (KVLQT1) knockout mouse: a model of Jervell and Lange-Nielsen syndrome. Otol. Neurotol. 26, 415–424.

Ryugo, D.K., Pongstaporn, T., Huchton, D.M., Niparko, J.K., 1997. Ultrastructural analysis of primary endings in deaf white cats: morphologic alterations in endbulbs of Held. J. Comp. Neurol. 385, 230–244.

Ryugo, D.K., Rosenbaum, B.T., Kim, P.J., Niparko, J.K., Saada, A.A., 1998. Single unit recordings in the auditory nerve of congenitally deaf white cats: morphological correlates in the cochlea and cochlear nucleus. J. Comp. Neurol. 397, 532–548.

Ryugo, D.K., Kretzmer, E.A., Niparko, J.K., 2005. Restoration of auditory nerve synapses in cats by cochlear implants. Science 310, 1490–1492.

Schmiedt, R.A., Mills, J.H., Boettcher, F.A., 1996. Age-related loss of activity of auditory-nerve fibers. J. Neurophysiol. 76, 2799–2803.

Schuknecht, H.F., 1994. Auditory and cytocochlear correlates of inner ear disorders. Otolaryngol. Head Neck Surg. 110, 530–538.

Siemens, J., Lillo, C., Dumont, R.A., Reynolds, A., Williams, D.S., Gillespie, P.G., Muller, U., 2004. Cadherin 23 is a component of the tip link in hair-cell stereocilia. Nature 428, 950–955.

Sobkowicz, H.M., Rose, J.E., Scott, G.E., Slapnick, S.M., 1982. Ribbon synapses in the developing intact and cultured organ of Corti in the mouse. J. Neurosci. 2, 942–957.

Spiwoks-Becker, I., Glas, M., Lasarzik, I., Vollrath, L., 2004. Mouse photoreceptor synaptic ribbons lose and regain material in response to illumination changes. Eur. J. Neurosci. 19, 1559–1571.

Spoendlin, H., Schrott, A., 1988. The spiral ganglion and the innervation of the human organ of Corti. Acta Otolaryngol. (Stockh) 105, 403–410.

Spoendlin, H., Schrott, A., 1990. Quantitative evaluation of the human cochlear nerve. Acta Otolaryngol. (Stockh) Suppl. 470, 61–70.

Stankovic, K., Rio, C., Xia, A., Sugawara, M., Adams, J., Liberman, M., Corfas, G., 2004. Survival of adult spiral ganglion neurons requires erbB receptor signaling in the inner ear. J. Neurosci. 24, 8651–8661.

Taberner, A.M., Liberman, M.C., 2005. Response properties of single auditory nerve fibers in the mouse. J. Neurophysiol. 93, 557–569.

Taschenberger, H., Leao, R.M., Rowland, K.C., Spirou, G.A., von Gersdorff, H., 2002. Optimizing synaptic architecture and efficiency for high-frequency transmission. Neuron 36, 1127–1143.

Walmsley, B., Alvarez, F.J., Fyffe, R.E.W., 1998. Diversity of structure and function at mammalian central synapses. TINS 21, 81–88.

White, J.A., Burgess, B.J., Hall, R.D., Nadol, J.B., 2000. Pattern of degeneration of the spiral ganglion cell and its processes in the C57BL/6J mouse. Hear. Res. 141, 12–18.

Willott, J.F., Bross, L.S., 1990. Morphology of the octopus cell area of the cochlear nucleus in young and aging C57BL/6J and CBA/J mice. J. Comp. Neurol. 300, 61–81.

Willott, J.F., Bross, L.S., 1996. Morphological changes in the anteroventral cochlear nucleus that accompany sensorineural hearing loss in DBA/2J and C57BL/6J mice. Dev. Brain Res. 91, 218–226.